JOURNAL OF THERMOPHYSICS AND HEAT TRANSFER
Vol. 17, No. 3, July–September 2003

Flat Surface Film Cooling from Cylindrical Holes with Discrete Tabs

Hasan Nasir,* Srinath V. Ekkad,† and Sumanta Acharya‡
Louisiana State University, Baton Rouge, Louisiana 70803

The effect of discrete delta-shaped tabs on film cooling performance from a row of cylindrical angled holes is investigated. The holes are inclined at 35 deg along the streamwise direction. Four tab locations are investigated: 1) tabs placed along the upstream edge of the hole covering 33% of the hole, 2) tabs placed along the upstream edge covering 11% of the hole, 3) tabs placed along the downstream edge of the hole, and 4) tabs placed along the lateral edges of the hole. They are compared to the baseline case without tabs. Measurements were carried out in a low-speed wind tunnel using the transient liquid crystal technique. The mainstream velocity and freestream turbulence intensity in the low-speed wind tunnel are 8.5 m/s and 6%, respectively, and the Reynolds number based on hole diameter is 6375. Three blowing ratios of 0.56, 1.13, and 1.7 are tested. Results show that the tab placed upstream of the hole covering 33% of the hole exit provides the highest film effectiveness compared to other tab locations studied. This is because the jet liftoff in the presence of the upstream tabs is reduced and there is greater lateral spreading of the jet.

Nomenclature

C_d = film hole discharge coefficient
d = film hole diameter, mm
h = heat transfer coefficient with film injection, W/m^2 · K
h_0 = heat transfer coefficient without film injection, W/m^2 · K
$\bar{\bar{h}}$ = spanwise averaged heat transfer coefficient
$\bar{\bar{h}}$ = area-averaged heat transfer coefficient
I = momentum flux ratio, $(\rho U^2)_c/(\rho U^2)_\infty$
k = thermal conductivity of test surface, W/m · K
k_a = thermal conductivity of air, W/m · K
l = height of the delta tab in the streamwise direction, cm
M = blowing ratio, $(\rho U_0)/(\rho U)_\infty$
Pr = Prandtl number
Re = Reynolds number, $\rho U_\infty d/\mu$
T = temperature, K
Tu = free stream turbulence intensity
t = time of liquid crystal color change, s
U = flow velocity, m/s
X = streamwise distance, m
y = spanwise distance, m
α = thermal diffusivity of test surface, m^2/s
γ = streamwise angle of film hole
η = film effectiveness, $(T_f - T_\infty)/(T_c - T_\infty)$
$\bar{\eta}$ = spanwise average film effectiveness
$\bar{\bar{\eta}}$ = area-averaged film effectiveness
μ = fluid dynamic viscosity, N · s/m^2
ρ = fluid density, kg/m^3
Φ = overall cooling effectiveness, $(T_\infty - T_w)/(T_\infty - T_c)$

Subscripts

c = coolant
f = film or adiabatic wall temperature
i = initial
w = wall
∞ = mainstream

Received 29 October 2002; revision received 24 March 2003; accepted for publication 24 March 2003.

*Graduate Assistant, Mechanical Engineering Department.
†Assistant Professor, Mechanical Engineering Department; ekkad@me.lsu.edu. Member AIAA.
‡LR Daniel Professor, Mechanical Engineering Department. Member AIAA.

Introduction

FILM cooling is used extensively in modern gas turbine engines for cooling hot gas path components such as airfoils. Injecting cooler air through discrete holes from inside the blade surface provides a coolant film that protects the outer blade surface from detrimental effects of the hot combustion gases. The holes are inclined along the streamwise direction at very shallow angles (around 30 deg) to provide high cooling effectiveness. Film cooling is highest when the coolant flow hugs the surface and does not penetrate and dissipate in the hot mainstream.

There are numerous studies that focus on film cooling over flat surfaces with streamwise coolant injection. Recently, efforts have been directed at exploring techniques that would enable enhanced film cooling effectiveness. Several studies[1–6] have focused on compound angle injection with cylindrical holes to provide increased cooling effectiveness. These studies show that compound angle injection provides higher film cooling effectiveness but also increases heat transfer coefficient in the region downstream of the jet. Sen et al.[3] and Schmidt et al.[4] presented some results with shaped holes. The shaped holes provide higher effectiveness and lower heat transfer coefficients compared to compound angle injection holes. Other studies[7] also show that shaped holes provide better film cooling protection. Hole shaping provides 30–50% higher film effectiveness and about 20% lower heat transfer coefficients on the surface compared to a typical cylindrical hole at the same blowing ratio. Shaped holes tailor the mainstream–jet interactions by reducing the jet momentum (keeping the mass flow rate constant). The resulting jets have lower penetration, thus, producing higher film effectiveness and lower heat transfer coefficients.

In recent years several studies have explored the effect of locating a tab at the exit of a jet injecting into a crossflow. It is well recognized that jet penetration into the crossflow is controlled by the evolution and growth of a kidney-shaped counter-rotating vortex pair (CVP). Tabs produce streamwise vorticity (vortex pair) in their wake and can beneficially or adversely interact with the jet CVP. Bradbury and Khadem[8] placed square tabs at the exit of a hole injecting vertically into the crossflow and examined their effects on the mixing phenomenon in the flowfield downstream of the holes. Zaman and Foss[9] and Zaman[10] also placed delta-shaped vortex generators upstream of the hole injected vertically into the crossflow and investigated their effects on the downstream flowfield. They reported a 40% reduction in jet penetration. Their tab was triangular

in shape and placed such that the apex of the triangle was tilted either up or down into the jet hole exit. They reported greater lateral spreading for the downward-tilted tab. However, all of the cited studies on using tabs to improve coolant protection were performed on jets with normal injection. Also, only flowfield measurements were presented, without any information on the heat transfer or film cooling effectiveness obtained with these geometries.

Most turbine blade geometries typically use angled injection to improve film cooling effectiveness. In this study, the focus is on injection holes angled at 35 deg along the streamwise direction. Discrete tabs were placed around the holes to improve film cooling performance. Whereas issues pertaining to manufacturability, costs, and reliability of the tabs in the harsh turbine environments can be raised, and are extremely important issues, the present study is limited to providing a proof of concept to the idea of using tabs for improving film cooling effectiveness. Later studies will address the mentioned practical issues pertaining to the integration of the concept for engine applications. Also, this study does not incorporate the density ratio effects that exist in the real engine because both coolant and mainstream are both at similar temperature levels.

Detailed heat transfer coefficients and film effectiveness distributions on the cooling surface with comparisons to typical cylindrical injection hole cases are presented. The tests are conducted on a flat surface with a single row of inclined cylindrical holes in a low-speed wind tunnel with compressed air supply for coolant air. Heat transfer measurements were made using a transient liquid crystal technique. Ekkad et al.[5,6] have demonstrated the effective use of a transient liquid crystal method for simultaneous determination of heat transfer coefficient and film effectiveness distributions.

Experimental Setup and Procedure

Figure 1 shows the comprehensive view of the experimental arrangement. The test setup consists of a blower connected to a 12-kW heater that heats the air to a freestream temperature of 58°C. The air is then routed through a section with baffles to ensure adequate mixing of the hot air to obtain a uniform temperature across the cross section. The presence of the baffles inadvertently contributed to the high freestream turbulence in the mainstream. A thermocouple was traversed across the test section to check for uniformity of the inlet thermal field. The air is then passed through a two-dimensional 4:1 converging nozzle. To allow the air to heat up to the desired temperature, the air exiting the nozzle is initially routed out away from the test section by using a bypass gate. The temperature of the air is continuously monitored at the exit of the gate, and when the desired temperature is reached, the gate is fully opened. The hot air is effectively sealed such that no air leaks into the test section and affects the initial temperature condition of the test surface. The open gate allows the flow into a test section made of Plexiglas® and has a cross section of 30 cm width and 9 cm height. The components upstream of the test section are covered with insulation to minimize the heating time. The bottom plate of the test section is made of 2.22-cm-thick Plexiglas. This plate has a replaceable section about 25.4 cm downstream of the test section inlet. This replaceable section can be interchanged to change the hole geometry. A trip is placed at the entrance to the test section to produce a fully turbulent boundary layer over the test plate. The film holes are located 30.5 cm downstream of the trip. The coolant air is provided from a separate compressed air supply and is metered for flow measurement. Air is then passed through a heater to heat up the air. Before the experiment, the hot air is routed away from the test section using a three-way diverter valve. When the valve is flipped, the coolant enters a plenum below the test plate and is then ejected through the film cooling holes into the test section. Thermocouples are mounted upstream of the hole row to measure the mainstream temperature and inside one of the holes to measure the coolant exit temperature. The coolant temperature is measured inside only one hole because pretesting showed that all film holes had the same flow rate and temperature conditions.

Figure 2 shows the test plate with film hole geometry used in this study. There are six holes of 1.27 cm diameter in each row. The

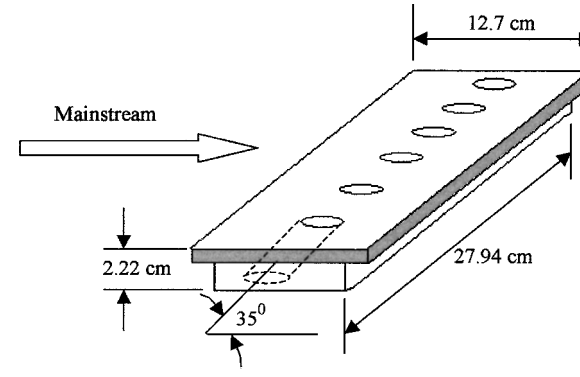

Fig. 2 Test plate geometry.

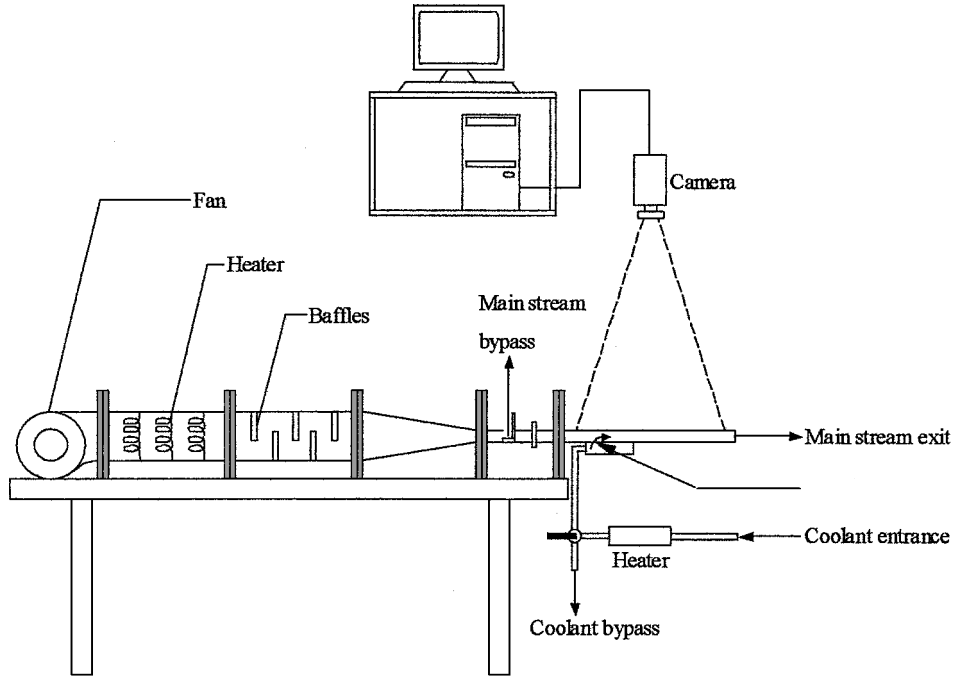

Fig. 1 Experimental setup.

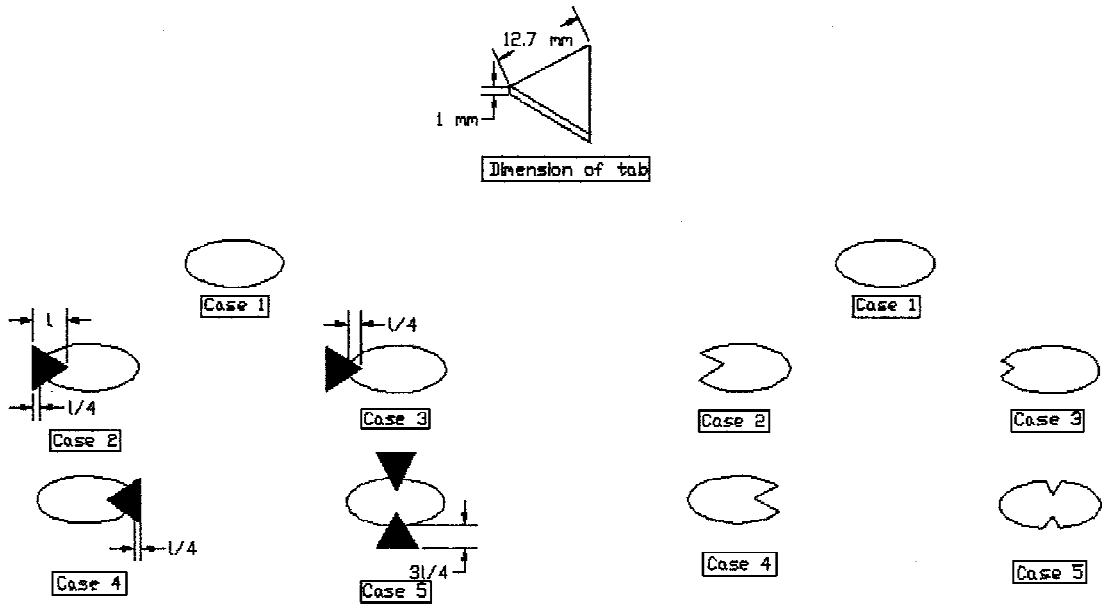

Fig. 3 Film hole geometry and tab placement.

hole spacing between adjacent holes is 3-hole diameters for all of the holes. Figure 3 shows the tab dimensions. The tab is a thin equilateral triangle made of cardboard material. The tabs are attached on to the surface using double-sided tape. The thickness of the tab is only 1 mm, which is negligible compared to the local boundary-layer thickness, $\delta = 9.7$ mm. Each side of the triangular piece is 1.27 cm, and the height of the tab, l, is 1.1 cm. The tabs are placed in the locations as shown in Fig. 3. Case 1 is the plain cylindrical hole with no tabs. In case 2, the tab is placed on the upstream side of the hole with the tab covering 33% ($3l/4$) of the upstream centerline length of the hole. Case 3 is where the tab covers only 11% ($l/4$) of the upstream centerline length of the hole. Case 4 is where the tab covers 33% of the downstream side of the hole. Case 5 is where two tabs are placed at the midsection of the holes such that the tabs cover the center region of the holes creating two distinct regions along upstream and downstream edges. The tabs cover 22% ($l/4$ for each tab) of the centerline area in the lateral direction. Figure 3 also shows the hole geometry the tabs effectively produce. In effect, these tabs modify the hole exit shape and produce shaped holes of a different form than that mentioned earlier.

The detailed velocity and turbulence measurements were obtained using a calibrated single hot wire and a TSI data acquisition system. These measurements were made to explore the effect of the tabs on the jet penetration and turbulence levels.

The liquid crystal color changes were digitized using an image processing system. The red–green–blue camera is placed above the test section and is connected to the color frame grabber board inside the computer. The frame grabber board is programmed through commercially available software to monitor the color change times of the liquid crystal coating. The software tracks the appearance of the green color (from test initiation) at every pixel location during a sudden transient heating experiment. More details on the measurement technique are provided by Ekkad et al.[5] Two tests with different coolant temperatures are run to resolve the heat transfer coefficient and film effectiveness at every pixel location. An 8-channel A/D system is used for measuring the temperatures during the transient test. Before the actual tests are conducted, the liquid crystal color is calibrated vs temperature to use the correct condition to calculate the heat transfer coefficient. Calibration is performed in situ using a thermocouple attached to the liquid crystal layer. The liquid crystal coating (R35C1W) has a temperature bandwidth of 1°C from red appearance to blue appearance. Green color appears at 35.4°C under the present test conditions.

The first test has the mainstream heated to 58°C and the coolant heated slightly above room temperature. Both the flows are initially heated and routed away from the test section. The airflow is suddenly switched to start a transient heating of the liquid crystal coating. The image processing system and the temperature measurement system are triggered to start obtaining data at the same instant that both coolant and main flows are switched into the test section. The time of color change of each pixel location to change color to green since the initiation of the transient test is determined. The second test is run similarly with the coolant temperature heated to a temperature slightly above the mainstream temperature. Both the heat transfer coefficient and film effectiveness are solved from the two equations simultaneously. For this study, there are 400 points (pixels) along the streamwise direction and 200 points (pixels) along the lateral direction. The measured region focuses on the four middle holes of the test section. The end holes are omitted due to wall effects. Typical test times are 80–120 s depending on the levels of heat transfer to the liquid crystal layer.

The generalized equation for the film cooling problem using semi-infinite solid assumption and one-dimensional transient conduction model is given as

$$T_w - T_i = \left[1 - \exp(h^2\alpha t/k^2)\,\mathrm{erfc}\left(h\sqrt{\alpha t}/k\right)\right] \times [\eta T_c + (1-\eta)T_\infty - T_i]$$

where T_w is the liquid crystal color change temperature (35.4°C). The transient responses of the mainstream and coolant temperatures during the tests are incorporated using Duhamel's superposition theorem. Subsequently, the two equations with different coolant temperatures and color change times are solved simultaneously to determine the local heat transfer coefficient and film effectiveness values at every single point on the test surface. More details of this solution technique are presented in Refs. 5 and 6.

As shown by Ekkad et al.,[6] the local heat flux ratio q''/q_0'', the heat flux with film injection to that without film injection, can be expressed as $q''/q_0'' = h/h_0[1 - (\eta/\Phi)]$, where h/h_0 and η are the measured area-averaged heat transfer coefficient and film effectiveness values, respectively. The values downstream of the holes are averaged over the entire measured region to produce singular values of h/h_0 and η. These values are then incorporated into the preceding equation to determine and overall-averaged heat flux reduction value for that particular cooling hole geometry. The value of Φ, the overall cooling effectiveness, is set at 0.6, which is a typical value for an actual turbine blade under engine conditions. A heat flux ratio of less than 1.0 indicates that film injection reduces the heat flux into the surface.

The average experimental uncertainty in heat transfer coefficient and film effectiveness measurement is estimated to be about ±6.9% and ±8.4%, respectively using the methodology of Kline and

McClintock.[11] The individual uncertainties in color change time t is ± 0.2 s, color change temperature calibration T_w is $\pm 0.2^\circ$C, mainstream temperature T_∞ is $\pm 0.2^\circ$C, surface initial temperature T_i is $\pm 0.2^\circ$C, coolant temperature T_c is $\pm 0.2^\circ$C, and material physical properties $\sqrt{\alpha/k}$ is $\pm 3\%$. Note that the uncertainty for heat transfer coefficient and film effectiveness in the immediate vicinity of the film hole could be as high as $\pm 10\%$ and $\pm 17\%$, respectively, due to short color change time or edge (two-dimensional conduction) effects. Experimental uncertainty in flow velocity and turbulence intensity measurements are on the order of $\pm 4\%$.

Results and Discussion

Velocity Measurements

The measured mainstream velocity and freestream turbulence using a calibrated single hot-wire probe are 8.5 m/s and 6%, respectively. The mainstream Reynolds number Re_d based on film hole diameter is 6750. The boundary-layer profile measured downstream of the trip is close to the fully turbulent flow profile (one-seventh law). The momentum thickness Reynolds number Re_θ just upstream of the hole is 511, and the corresponding boundary-layer thickness is 9.87 mm. Three blowing ratios, $M = 0.56$, 1.13, and 1.7, are tested for cases 1, 2 and 4. Cases 3 and 5 are tested only at $M = 1.13$. The blowing ratios represent unblocked hole case values. In all other cases, the mass flow rate was maintained as in the case of the fully open hole. This helped in the comparison because equal mass flow rate would be expected out of the blocked and unblocked holes.

Figure 4 presents the velocity profiles upstream of the hole, $X/d = -1$, and at several locations downstream of the hole, $X/d = 1, 3, 5$, and 10. These velocity profiles are presented for a representative $M = 1.13$. The upstream velocity profile at $X/d = -1$, as indicated earlier, is typical of a turbulent boundary layer with one-seventh law profile and is relatively unaffected by the jet injection. The no-tabs (case 1) velocity profile shows an inflection due to the coolant jet just downstream of injection at $X/d = 1$ with the highest velocity around $Y/d \sim 0.8$. Farther downstream, the jet injection effect reduces rapidly, and the flow begins to recover. However, as far downstream as $X/d = 10$, the velocity profile indicates that the flow recovery is not yet complete. For case 2 (upstream tabs with 33% blockage), the location of peak velocity is closer to the wall (peak velocity location at $Y/d \sim 0.5$), indicating that the jet penetration is reduced in the presence of the tabs. With the tabs located upstream of the hole center, a vortical pair with vorticity opposite to that of the jet–kidney vortices are obtained by Zaman[10] and reduce the strength of the kidney vortices. This reduces the self-induction of vorticity and the jet penetration. This should lead to improved film cooling effectiveness (presented in the next section). The lower jet penetration can also be observed at $X/d = 3$. For case 3 (upstream tabs with 11% blockage), the point of inflection is farther away from the wall (peak velocity location at $Y/d \sim 0.8$) than case 2, and the coolant jet velocity at $X/d = 1$ is lower. Clearly, the blockage ratio of the tabs is an important parameter in controlling the jet penetration. For case 4 (tabs located at the downstream edge of the hole), the velocity peak at $X/d = 1$ occurs at a higher Y/d location ($Y/d \sim 1$–1.1) relative to cases 1–3. This is also evident in the velocity profile at $X/d = 3$, where the peak velocity location is shifted upward ($Y/d \sim 1.3$) relative to the location ($Y/d \sim 1$) for case 1 or 3. The greater jet penetration is expected to be detrimental for film cooling effectiveness. With case 5 (tabs located along the spanwise edges of the hole), the velocity peak at $X/d = 1$ is at a similar location as for case 4. However at $X/d = 3$, the peak location is at $Y/d = 1.5$ and shows that, for this configuration, the jet penetration appears to be the highest. Therefore, one would expect that this case would not perform well from the perspective of film cooling effectiveness.

Figure 5 shows the mixed stream turbulence intensity upstream at $X/d = -1$ and at several locations downstream of the hole, $X/d = 1$, 3, 5, and 10. Several studies have shown that jet injection produces increased turbulence levels inside the boundary layers due to the shear layer mixing and that this is the main reason that the local heat transfer coefficients downstream of jet injection show higher values. To improve blade cooling, the cooling effectiveness must be

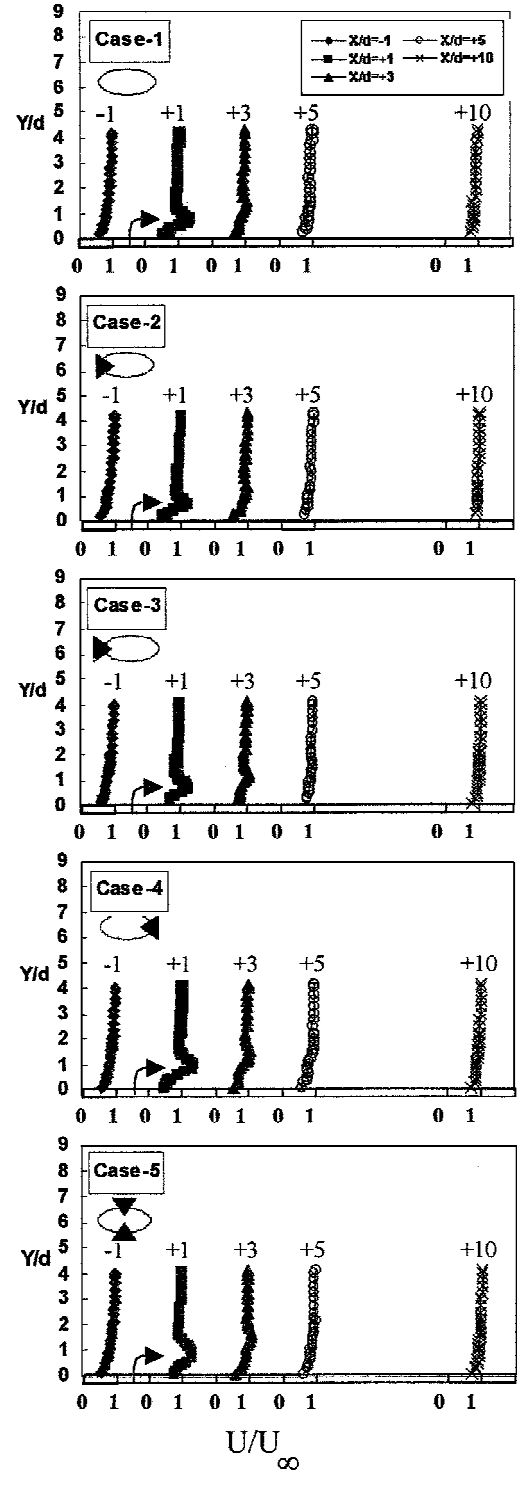

Fig. 4 Velocity profile measurements upstream and downstream of coolant injection.

increased without affecting the surface heat transfer coefficients. In Fig. 5, the maximum turbulence intensities will be interpreted as a measure of the turbulent mixing produced by the presence of tabs. For the no-tabs condition (case 1), the maximum turbulence intensity at $X/d = 1$ is around 25%. The profiles show two peaks, and these represent the wake region (peak closer to the wall) and the jet (peak closer to the freestream). The effect of these separate origins can be seen as far downstream as $X/d = 5$. Note that the cross-flow boundary layer is entrained into the wake region and leads to high-turbulence-intensity levels in this region. The peak turbulence intensity for the case 2 tab is only slightly higher (27%) than that for the no-tab conditions, indicating that the presence of the upstream

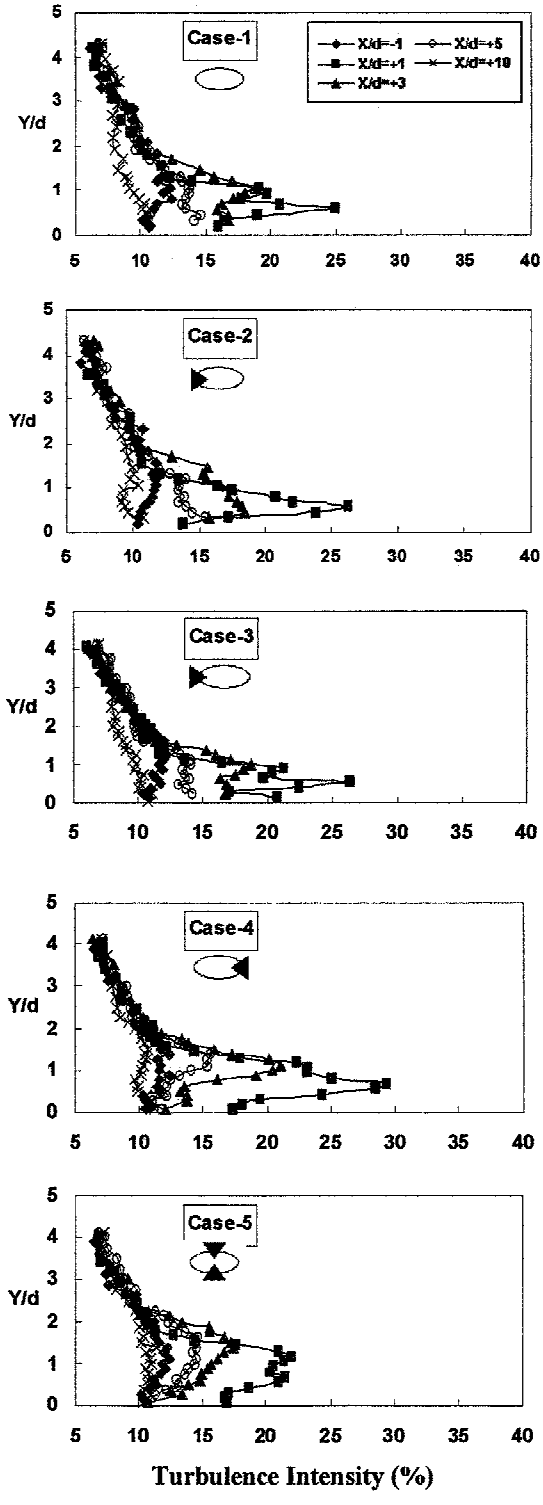

Fig. 5 Turbulence intensity measurements upstream and downstream of coolant injection.

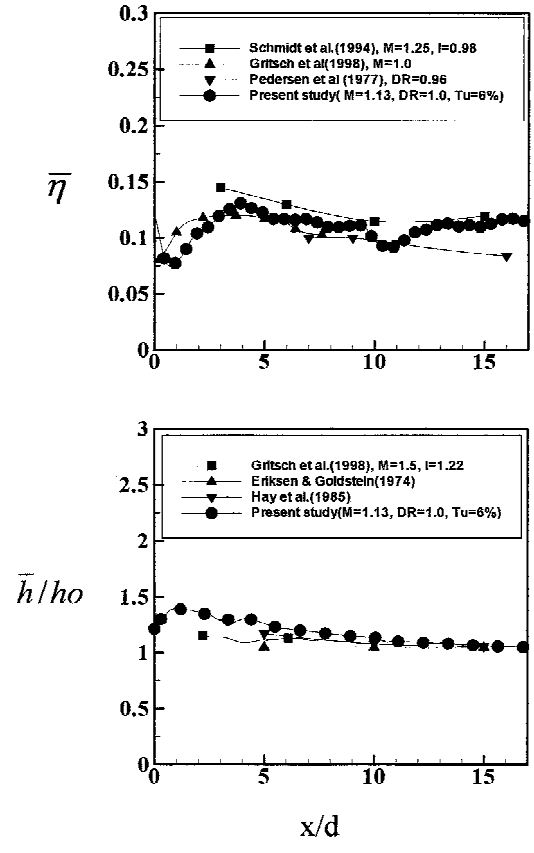

Fig. 6 Comparison of present data with other studies.

tab does not considerably enhance the shear layer mixing. However, as pointed out earlier, the jet is somewhat closer to the surface. The greater proximity of the jet to the wall is likely to lead to enhanced effectiveness as seen later. Furthermore, the slight increase in the intensity levels, as well as the greater proximity of the peak velocity to the wall, is also likely to increase the heat transfer coefficient. The turbulence intensity for case 3 is similar to that for case 2 with values close to 25%. The peak turbulence intensity increases for the downstream tabs (case 4) with values close to 30%. This may be a reflection of the closer proximity of the downstream tabs to the wake region. However, as observed in the mean velocity plots (Fig. 4), the location of the peak turbulence intensity is slightly shifted away from the wall. The upward shift in the peak velocity location is likely to reduce film cooling effectiveness, whereas the increased turbulence intensity levels are likely to increase heat transfer coefficient. For case 5, the peak intensity is reduced and is displaced farther away from the wall. Both of these effects are expected to produce a decrease in the heat transfer coefficient.

Heat Transfer and Cooling Effectiveness

Figure 6 presents the comparison of the present results with published results for $M = 1.13$ for simple injection holes (case 1). The spanwise-averaged film effectiveness $\bar{\eta}$ results for $M = 1.13$ are compared with the results from Pedersen et al.[12] for $M = 1.0$, Schmidt et al.[4] for $M = 1.25$, and Gritsch et al.[8] for $M = 1.0$ in Fig. 6a. Results show that the present data for $M = 1.13$ are in good agreement with results from all the cited studies. The data from Gritsch et al.[8] also show the slight increase in film effectiveness just downstream of the holes. Other studies do not present data close to the hole. The spanwise-averaged ratio $(\bar{h}/h_0)$ of the local heat transfer coefficient with film injection h normalized by the local heat transfer coefficient without film holes h_0 is plotted in Fig. 6b for $M = 1.13$, and the present results are compared with those of Eriksen and Goldstein[13] for $M = 1.0$, Hay et al.[14] for $M = 1.0$, and Gritsch et al.[7] for $M = 1.5$. The present data compare well with the other studies. The results from the other studies are beyond $X/d = 5$, whereas the present study shows near-hole results. Based on the preceding comparisons, it is fair to say that the results from the present study are in good agreement with published results for the baseline case.

Figure 7 shows the detailed film cooling effectiveness distributions η for all cases at $M = 1.13$. The detailed distributions are shown for only the two middle holes. For case 1, the film effectiveness distributions are higher along the jet centerlines, with almost no cooling in between the holes for most of the plate length. The jets appear to lift off at the downstream edge and reattach farther downstream, creating a low effectiveness region just downstream of the holes. After reattachment, the jets spread laterally. Case 2 shows

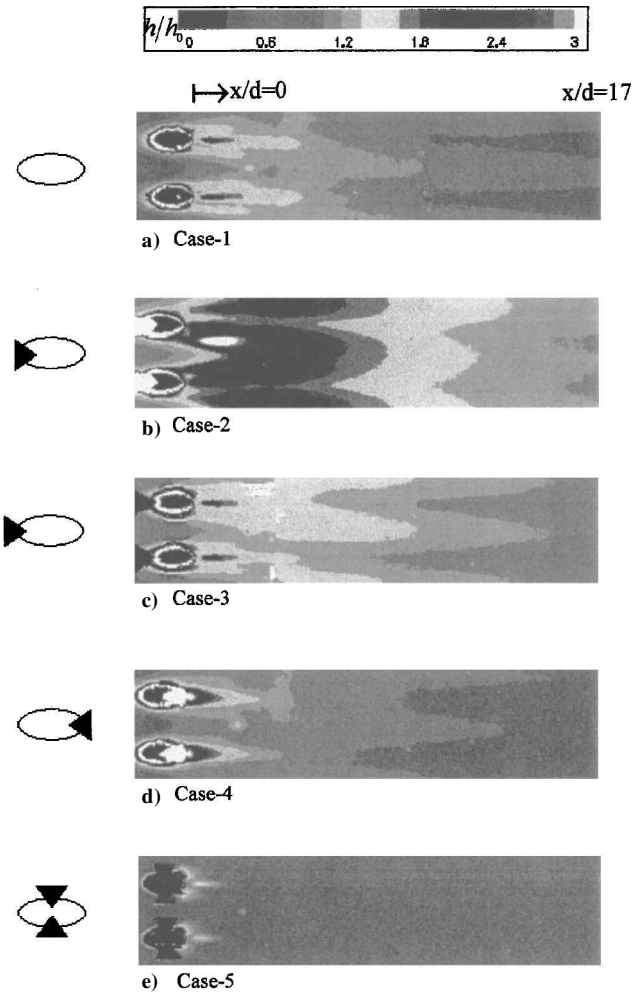

Fig. 7 Detailed film effectiveness distributions for all cases.

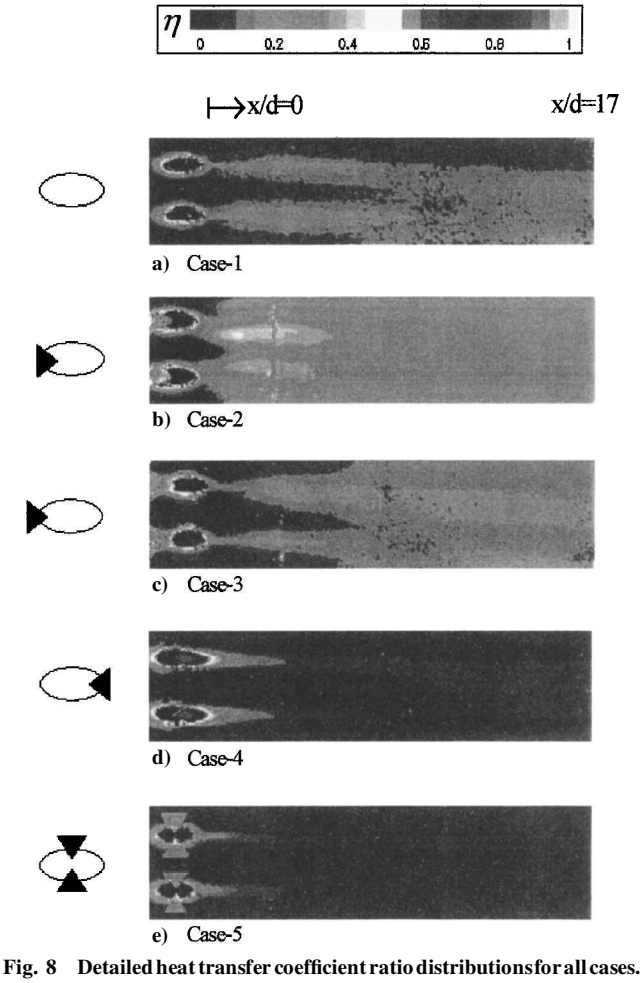

Fig. 8 Detailed heat transfer coefficient ratio distributions for all cases.

much higher effectiveness than case 1 over the entire region. Furthermore, complete coverage is achieved within 2-hole diameters. As noted earlier in Fig. 4, with the tabs located upstream of the hole center, the jet penetration is reduced due to tab-generated vorticity countering the kidney vortices. Because the penetration of the coolant jet is reduced, higher film cooling effectiveness and greater coverage are obtained. The rapid increase in the coverage is also indicative of the jet spreading. Case 3 also uses an upstream tab, but the blockage is not as high (11%) as case 2 (33%). The effectiveness values and lateral coverage are considerably higher than the baseline case, but lower effectiveness is obtained relative to case 2. Therefore, it appears that the blockage of the hole is an important parameter and that the higher blockage (33%) provides greater reduction in the jet penetration and higher film cooling effectiveness. Case 4, corresponding to the downstream located tab, exhibits considerably lower cooling effectiveness compared to cases 1–3, except in the very near vicinity of the tabs. Recall that, for case 4, greater jet penetration had been observed in Fig. 4, and this leads to lower effectiveness. The lower film effectiveness for the downstream tabs are consistent with the observations of Zaman and Foss,[9] who linked the ineffectiveness of the tabs to the existence of a pressure valley that cancels or reduces the strength of the tab-generated vortices. Case 5, where the tabs are located along the spanwise edges of the jet hole, produces almost no cooling effectiveness on the surface. The jet structure lifts off to a greater degree than the other cases (as seen in Fig. 4), leading to no presence of the coolant film along the wall.

From the preceding observations, the highest effectiveness is clearly achieved with the upstream-located tabs. Tabs located downstream, and along the spanwise edges of the jet, degrade the effectiveness over the baseline case.

Figure 8 shows the detailed heat transfer coefficient ratio distributions (h/h_0) for all cases at $M = 1.13$. The heat transfer coefficient distributions for the case 1 are consistent with the distributions presented by Goldstein and Taylor.[15] The region along the centerline shows a low heat transfer region behind the downstream edge of the hole. This is potentially due to the action of jet liftoff and flow separation downstream of the jet. Farther downstream, the heat transfer coefficient ratio is enhanced beyond values of 2.0. Case 2 shows much higher heat transfer coefficient ratios compared to case 1. As noted earlier, in case 2, the tab-induced vorticity reduces the jet vertical penetration and also appears to increase the lateral spreading. Slightly higher turbulence intensities were noted for this case (Fig. 5), which imply greater levels of jet–crossflow mixing close to the wall. This fact and the reduced penetration that increases the velocities near the wall produce higher values of the measured heat transfer coefficients. Case 3 shows lower heat transfer coefficient ratios and also less spreading than case 2. However, the values are higher than that for case 1. These observations are also consistent with the film cooling effectiveness results, as shown in Fig. 5. With the tab on the downstream edge (case 4), jet penetration is increased, as noted earlier, but the turbulence intensity in the wake region in the near vicinity of the tabs is considerably greater (Fig. 5). Thus, the heat transfer coefficient ratios immediately downstream of the tabs are considerably higher than the baseline case. Farther downstream, due to the increased jet penetration, the heat transfer coefficients decay rapidly. For case 5, the jet liftoff is considerably greater than the baseline (as seen in Fig. 4), and turbulence intensities are much lower than cases 1–4. Therefore, this case is associated with the lowest heat transfer coefficient.

Figure 9 presents the effect of blowing ratio, M, on the spanwise-averaged film effectiveness $\bar{\eta}$ and heat transfer coefficient ratio ($\bar{h}/h_0$) distributions for a plain hole (case 1). The averaged data obtained for the entire region consist of four holes. Film effectiveness is highest for $M = 1.13$ for most of the test section. Effectiveness is lowest for $M = 1.7$ just downstream of the hole due to jet liftoff and reattachment. In the region $X/d > 9$, all three blowing

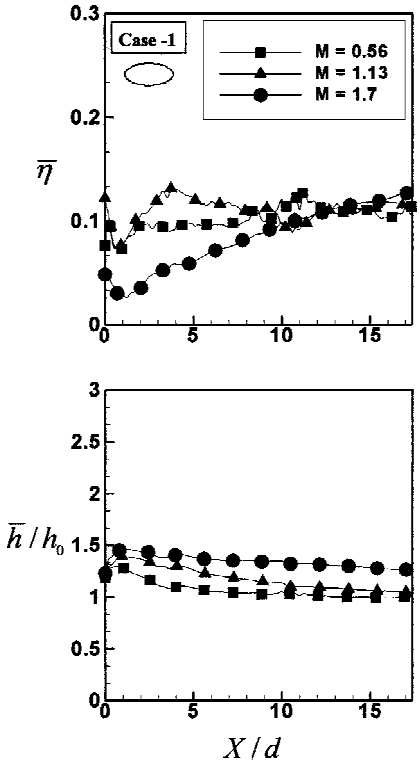

Fig. 9 Effect of blowing ratio on span-averaged film effectiveness and heat transfer coefficient ratio distributions for case 1.

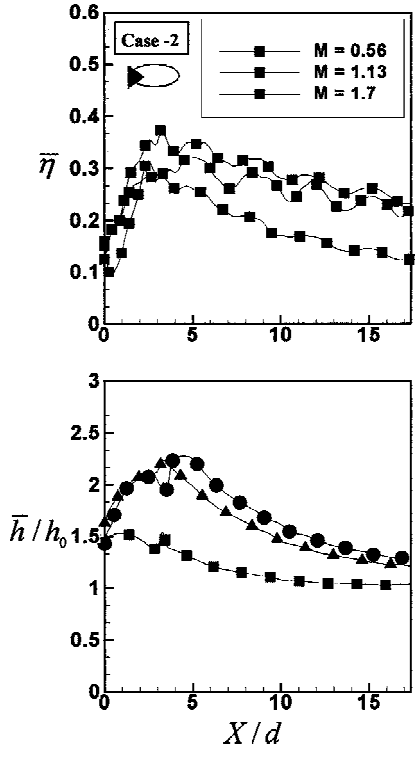

Fig. 10 Effect of blowing ratio on span-averaged film effectiveness and heat transfer coefficient ratio distributions for case 2.

ratios provide similar levels of film effectiveness. The highest effectiveness is around 0.13 for this hole geometry for any blowing ratio. As expected, the heat transfer coefficient ratios increase with increasing blowing ratio. The increased coolant injection typically produces increases in mixing and turbulence generation, resulting in higher heat transfer coefficients.

Figure 10 shows the effect of blowing ratio, M, on spanwise-averaged film effectiveness $\bar{\eta}$ and heat transfer coefficient ratio

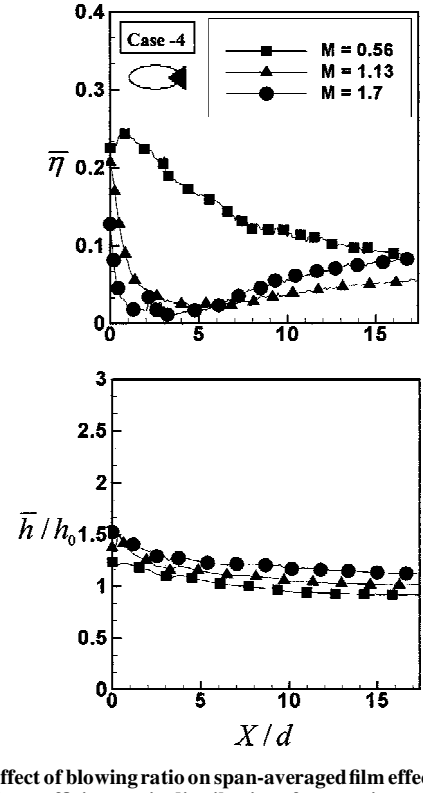

Fig. 11 Effect of blowing ratio on span-averaged film effectiveness and heat transfer coefficient ratio distributions for case 4.

$(\bar{h}/h_0)$ for case 2. Effectiveness is significantly higher at all blowing ratios for case 2 compared to case 1. The jets seem to reattach around $X/d \sim 3$–4 for all blowing ratios. Highest effectiveness of around 0.35 is obtained for blowing ratio of $M = 1.13$. Effectiveness is lowest for $M = 0.6$, where the jet spreading is limited due to lower coolant mass flux. The heat transfer coefficient ratios are also higher for case 2 compared to case 1. As noted earlier, the increased turbulence and mixing and higher near-wall velocities for this case also produces higher heat transfer coefficients. There is a significant increase in heat transfer coefficient as M increases from 0.56 to 1.13, but the heat transfer coefficient is not significantly affected with further increases in M to 1.56.

Figure 11 presents the effect of blowing ratio, M, on spanwise averaged film effectiveness $\bar{\eta}$ and spanwise-averaged heat transfer coefficient ratio $(\bar{h}/h_0)$ for case 4. The tab is on the downstream edge of the hole for this case. Effectiveness is significantly high at $M = 0.56$, but there is almost no cooling effectiveness for higher blowing ratios. The jet penetration for this case is higher, and there may be increased dispersion of the jet for higher blowing ratios, leading to lower effectiveness. Therefore, this geometry is effective only at low blowing ratios. However, note that the levels of heat transfer coefficient enhancement are not as high as case 2.

Figure 12 show a comparison of the hole geometry effect on spanwise-averaged film effectiveness $\bar{\eta}$, heat transfer coefficient ratio $(\bar{h}/h_0)$, and heat flux ratio (q''/q''_0) for all five cases at $M = 1.13$. It is clearly evident that case 2 provides the highest effectiveness, with cases 4 and 5 providing negligible cooling. Cases 1 and 3 provide similar levels of effectiveness. Case 2 also produces significantly higher heat transfer coefficient enhancement compared to all of the other cases. Figure 12c shows the effect of both the heat transfer coefficient enhancement and film effectiveness combined and expresses the combination as a heat flux ratio $(\bar{q}''/q''_0)$. A heat flux ratio of less than 1.0 indicates that film cooling is beneficial. Film effectiveness for case 2 is about 200% higher than that for the other four cases, and heat transfer coefficient ratio is about 25–30% higher than the other four cases. This produces about 30% lower heat flux ratio for case 2 at $M = 1.13$ compared to other cases for the region $X/d > 4$. Thus, in case 2, the increase in heat transfer coefficient is clearly offset by the significant enhancement in cooling

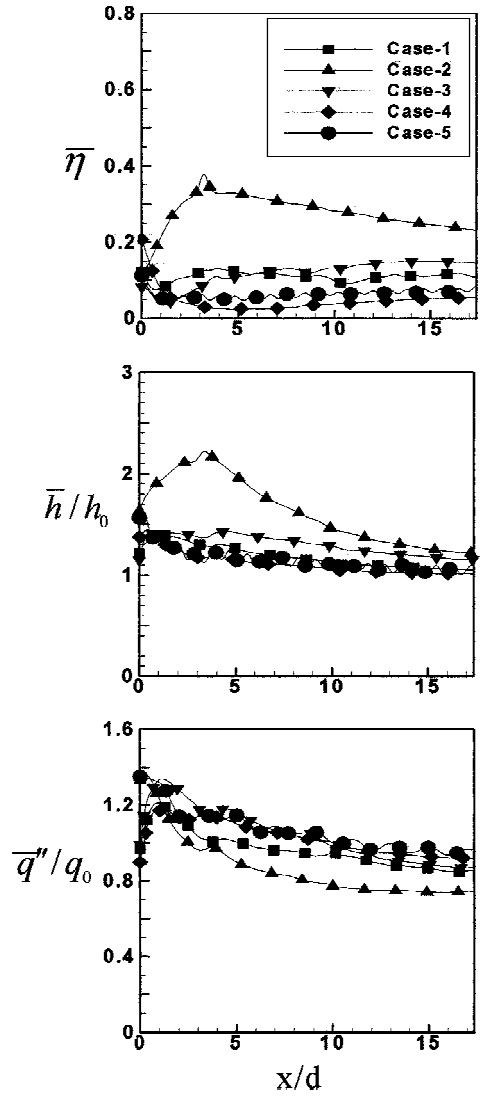

Fig. 12 Effect of tab placement on span-averaged film effectiveness, heat transfer coefficient ratio, and heat flux ratio distributions for $M = 1.13$.

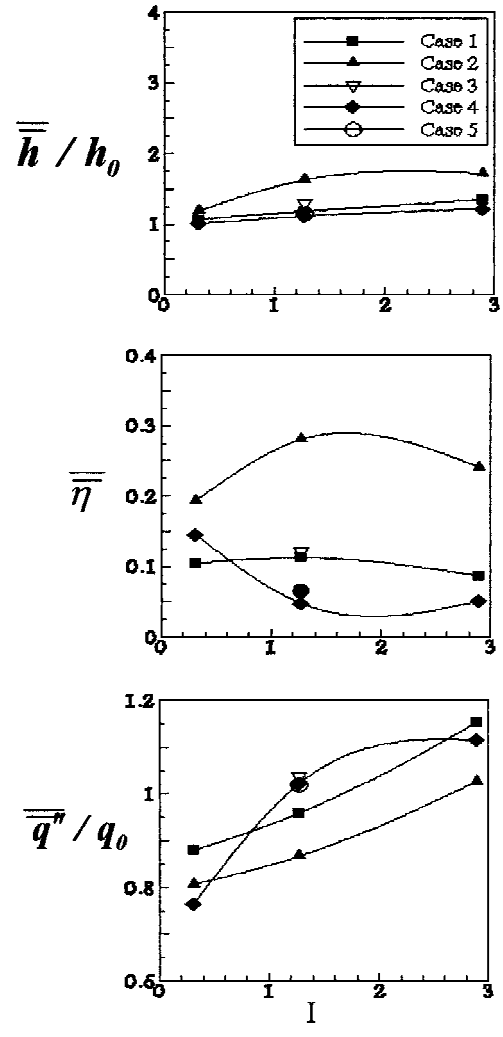

Fig. 13 Effect of momentum flux ratio I on overall-averaged film effectiveness, heat transfer coefficient ratio, and heat flux ratio distributions.

effectiveness. The other four cases produce similar levels of heat flux ratios on most of the surface.

Figure 13 shows the effect of momentum flux ratio I on area-averaged heat transfer coefficient ratios ($\bar{h}/h_0$) and film effectiveness $\bar{\bar{\eta}}$ for each of the five cases. Cases 1, 2, and 4 are shown at all blowing ratios (all I), but cases 3 and 5 are presented for only $M = 1.13$. Cases 3 and 5 are shown as open symbols. Results show that the heat transfer coefficient ratios increase with increasing I for all cases. Case 2 consistently produces higher heat transfer coefficients, as earlier indicated. Case 2 also produces significantly higher film effectiveness levels compared to the other four cases. The plain hole (case 1) performs better than cases 4 and 5. Case 4 produces slightly higher effectiveness at low blowing ratios. When the heat transfer coefficient and film effectiveness values are combined, the heat flux ratio distributions ($\bar{q}''/q_0''$) show that case 2 produces heat flux ratios less than 1.0 for all blowing ratios. Case 1 also performs well at low blowing ratios. Case 4 provides significant heat flux reduction with film cooling for a low blowing ratio of $M = 0.56$, but does not perform well at high blowing ratios. Cases 3 and 5 show heat flux ratios around 1.0, indicating that these tab placements may not provide any benefit.

Discharge Coefficients

The discharge coefficients (inversely proportional to the pressure drop across the coolant hole) are plotted in Fig. 14. The discharge coefficients are shown both with and without the cross flow only

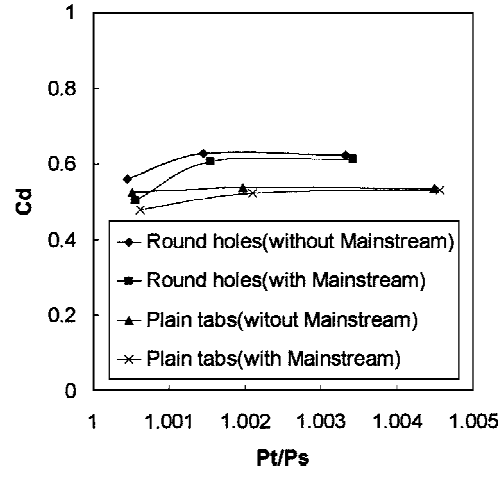

Fig. 14 Effect of upstream tab on discharge coefficients C_d with and without crossflow.

for the upstream tabs and show only a small effect of the crossflow at low-pressure ratios. There is a significantly larger pressure drop with the presence of tabs. Note that the horizontal tabs provide similar levels of discharge coefficients as that shown by Gritsch et al.[8] for their shaped holes at low-pressure ratios. This observation combined with the significantly greater cooling effectiveness achieved with cases 2 and 3 compared to the baseline case indicate the potential benefits of using tabs to enhance blade cooling. Most of the

data shown by Gritsch et al.[8] were for high-pressure ratios, and the present study investigates fairly low-pressure ratio conditions. These results may be applicable for film hole rows on the pressure surface of the blade near the leading-edge stagnation point.

Conclusions

The influence of placing a tab at the exit of a film cooling hole on the surface heat transfer coefficient and film effectiveness has been investigated. Four different tab placements have been tested. The tabs alter the jet exit structure producing varied jet–mainstream interactions that affect the heat transfer coefficient and film effectiveness distributions. The detailed heat transfer coefficient and film effectiveness distributions clearly indicate the jet spreading, liftoff, and reattachment phenomena due to the presence of the tabs. The results show that the tab located along the upstream edge of the hole enhances coolant coverage and increases film cooling effectiveness. A triangular tab that covers about 33% of the upstream hole area provides significantly more coolant spreading and increases film effectiveness over the entire surface by over 200% compared to the plain hole. There is also an associated increase in the jet–mainstream mixing, which leads to higher heat transfer coefficients. The other tab locations (located along the downstream edge and along the spanwise edges), in general, show lower film protection compared to the no-tab plain hole. In all, the tab placement should be on the upstream side of the hole and should not create strong blockage. The alteration of the flowfield should be relatively mild, thus, producing the right mix of improved coolant coverage and slightly higher undesired jet–mainstream mixing.

Acknowledgments

The authors acknowledge the support from the project funded by Louisiana Board of Regents through the NASA–Louisiana Space Consortium Research Enhancement Award under Contract NASA/LEQSF (1996-2001). The Program Manager is John Wefel.

References

[1]Ligrani, P. M., Wigle, J. M., Ciriello, S., and Jackson, S. W., "Film-Cooling From Holes with Compound Angle Orientations: Part 1—Results Downstream of Two Staggered Rows of Holes with 3d Spanwise Spacing," *Journal of Heat Transfer*, Vol. 116, No. 2, 1994, pp. 341–352.

[2]Ligrani, P. M., Wigle, J. M., and Jackson, S. W., "Film-Cooling From Holes with Compound Angle Orientations: Part 2—Results Downstream of a Single Row of Holes with 6d Spanwise Spacing," *Journal of Heat Transfer*, Vol. 116, No. 2, 1994, pp. 353–362.

[3]Sen, B., Schmidt, D. L., and Bogard, D. G., "Film Cooling with Compound Angle Holes: Heat Transfer," *Journal of Turbomachinery*, Vol. 118, No. 4, 1996, pp. 801–807.

[4]Schmidt, D. L., Sen, B., and Bogard, D. G., "Film Cooling with Compound Angle Holes: Adiabatic Effectiveness," *Journal of Turbomachinery*, Vol. 118, No. 4, 1996, pp. 807–813.

[5]Ekkad, S. V., Zapata, D., and Han, J. C., "Heat Transfer Coefficients Over a Flat Surface with Air and CO_2 Injection Through Compound Angle Holes Using a Transient Liquid Crystal Image Method," *Journal of Turbomachinery*, Vol. 119, No. 3, 1997, pp. 580–586.

[6]Ekkad, S. V., Zapata, D., and Han, J. C., "Film Effectiveness Over a Flat Surface with Air and CO_2 Injection Through Compound Angle Holes Using a Transient Liquid Crystal Image Method," *Journal of Turbomachinery*, Vol. 119, No. 3, 1997, pp. 587–593.

[7]Gritsch, M., Schulz, A., and Wittig, S., "Adiabatic Wall Effectiveness Measurements of Film Cooling Holes with Expanded Exits," *Journal of Turbomachinery*, Vol. 120, No. 3, 1998, pp. 549–556.

[8]Bradbury, L. J. S., and Khadem, A. H., "The Distortion of a Jet by Tabs," *Journal of Fluid Mechanics*, Vol. 70, No. 4, pp. 801–813.

[9]Zaman, K. B. M. Q., and Foss, J. K., "The Effect of Vortex Generators on a Jet in a Cross-Flow," *Physics of Fluids*, Vol. 9, No. 1, 1997, pp. 106–114.

[10]Zaman, K. B. M. Q., "Reduction of Jet Penetration in a Cross-Flow by Using Tabs," AIAA Paper 98-3276, June 1998.

[11]Kline, S. J., and McClintock, F. A., "Describing Uncertainties in Single Sample Experiments," *Mechanical Engineering*, Vol. 75, No. 1, 1953, pp. 3–8.

[12]Pedersen, D. R., Eckert, E. R. G., and Goldstein, R. J., "Film Cooling with Large Density Differences Between the Mainstream and the Secondary Fluid Measured by the Heat-Mass Transfer Analogy," *Journal of Heat Transfer*, Vol. 99, No. 4, 1977, pp. 620–627.

[13]Eriksen, V. L., and Goldstein, R. J., "Heat Transfer and Film Cooling Following Injection Through Inclined Circular Holes," *Journal of Heat Transfer*, Vol. 96, No. 3, 1974, pp. 239–245.

[14]Hay, N., Lampard, D., and Saluja, C. L., "Effect of Cooling Films on the Heat Transfer Coefficient on a Flat Plate with Zero Mainstream Pressure Gradient," *Journal of Engineering for Gas Turbines and Power*, Vol. 107, No. 1, 1985, pp. 105–110.

[15]Goldstein, R. J., and Taylor, J. R., "Mass Transfer in the Neighborhood of Jets Entering a Crossflow," *Journal of Heat Transfer*, Vol. 104, No. 4, 1982, pp. 715–721.